Supporting Information

Enhanced thermoelectric performance in high-defect SnTe alloys: a significant role of carrier scattering

Fu-Jie Zhang,[a] Xuan-Wei Zhao,[a] Rui-Heng Li,[a] Shan He,[a] Xiao-Bo Tan,[a] Jiang-Long Zhu,[a] and Ran Ang*[ab]

a Key Laboratory of Radiation Physics and Technology, Ministry of Education, Institute of Nuclear Science and Technology, Sichuan University, Chengdu 610064, China

b Institute of New Energy and Low-Carbon Technology, Sichuan University, Chengdu 610065, China

*Corresponding authors and Emails: rang@scu.edu.cn

Experimental section

Material synthesis.

Polycrystalline SnTe-$x$$Sb_2Te_3$ (x = 0, 0.02, 0.04, 0.06, 0.08, 0.1) and $Sn_{1-y}Cd_yTe$-$0.08Sb_2Te_3$ (y = 0.02, 0.04, 0.05, 0.06, 0.07) were synthesized by vacuum hot-melting the stoichiometric amounts of high-purity Sn (99.99%), Te (99.999%), Cd (99.99%), Sb (99.99%). These mixtures are vacuum-sealed in quartz tubes, which are slowly heated to 1173 K in a furnace after 400 minutes, and then quenched directly in cold water after holding for 18 hours. The quenched samples were annealed at 873K for at least two days. The obtained ingot was ground into powder for hot pressing. Dense pellet samples were obtained by rapid hot pressing at 853 K for 30 min under a uniaxial pressure of ~55 MPa, whose density d measured by Archimedes method and had not less than 96% of the theoretical density (**Table S1**).

Table S1. Density of all SnTe-$x$$Sb_2Te_3$ and $Sn_{1-y}Cd_yTe$-$0.08Sb_2Te_3$ samples in this work.

Composition	Measured Density (g cm^{-3})	Relative Density (%)
SnTe	6.398	97.40
SnTe-$0.02Sb_2Te_3$	6.292	98.06
SnTe-$0.04Sb_2Te_3$	6.271	97.07
SnTe-$0.06Sb_2Te_3$	6.270	97.06
SnTe-$0.08Sb_2Te_3$	6.257	96.86
SnTe-$0.10Sb_2Te_3$	6.254	96.81
$Sn_{0.98}Cd_{0.02}Te$-$0.08Sb_2Te_3$	6.261	96.92
$Sn_{0.96}Cd_{0.04}Te$-$0.08Sb_2Te_3$	6.321	97.85
$Sn_{0.95}Cd_{0.05}Te$-$0.08Sb_2Te_3$	6.279	97.20
$Sn_{0.94}Cd_{0.06}Te$-$0.08Sb_2Te_3$	6.289	97.35
$Sn_{0.93}Cd_{0.07}Te$-$0.08Sb_2Te_3$	6.315	97.76

Materials Performance Characterization

The powder X-ray diffraction patterns were recorded with Cu *Kα* radiation. Scanning electron microscope (SEM) equipped with energy-dispersive spectroscopy (EDS) was used to characterize surface morphology and qualitative and quantitative analysis of composition. The electrical conductivity σ and Seebeck coefficient S were measured by CTApro measurement system (Beijing Cryoall Science and Technology Co., Ltd. China). The Hall coefficient, which was closely related to carrier concentration and mobility, was measured using the van der Pauw technique under a reversible magnetic field of 1.5 T. The thermal conductivity (κ_{total}) was calculated by $\kappa=dC_pD$, where D is the thermal diffusivity measured by a laser flash technique with the Netzsch LFA467 system (**Fig. S6**), C_p is the heat capacity estimated by $C_p(k_B/atom)=3.07+4.7(T/K-300)/10000$.[1, 2] Ignoring the bipolar thermal conductivity (κ_{bip}), the lattice thermal conductivity (κ_l) was directly obtained by subtracting the electronic conductivity (κ_e) from the κ_{total}, the κ_e was calculated by the Wiedemann-Franz relationship (**Fig. S8**), $\kappa_e = LT/\rho$, where L is the Lorentz number.[3] L was derived with the single parabolic band (SPB) model (**Fig. S7**).[4]

The first principle calculations were performed by utilizing the Perdew-Burke-Ernzerhof (PBE) formalism and generalized gradient approximation (GGA) implemented in Vienna ab initio simulation package (VASP) code. The plane-wave basis was truncated at the energy cutoff of 600 eV.

Modeling study on electronic transport

The single parabolic (SPB) model: [5]

The Seebeck coefficient S:

$$S = \frac{k_b}{e}\left[\frac{(r + 5/2)F_{r+3/2}(\eta)}{(r + 3/2)F_{r+1/2}(\eta)} - \eta\right] \quad \text{(S1)}$$

where η is the reduced chemical potential, k_B is the Boltzmann constant, e is the electron charge, r is the scattering factor.

The carrier concentration n_H:

$$n_H = 4\pi\left[\frac{2m^* k_B T}{h^2}\right]^{3/2} F_{1/2} \quad \text{(S2)}$$

where m^* is the density of state effective mass taking into account band degeneracy, h is the Plank's constant, T is the absolute temperature.

The mobility μ_H:

$$\mu_H = \mu_0\frac{F_{-1/2}}{2F_0} = \frac{\tau_0 e F_{-1/2}}{m^* 2F_0} \quad \text{(S3)}$$

where τ_0 is the relaxation time that is closely related to the energy in the case of acoustic

phonon scattering:[6] $\tau_0 = \frac{h^4 C_l}{8\sqrt{2}\pi^3 E_{def}{}^2 m^* k T^{3/2}}$. Where C_l is a parameter determined by the combination of the elastic constant,[7] E_{def} is a combination of deformation potentials for multivalley systems.[8]

The Hall factor A:

$$A = \frac{3}{2}F_{1/2}(\eta)\frac{F_{-1/2}}{2F_0^2} \tag{S4}$$

The Hall factor reflects the energy scattering mechanism and the anisotropy of the energy band. For the SPB model, anisotropy does not need to be considered.

The Lorenz number L:

$$L = \frac{\kappa_B^2 3F_0F_2 - 4F_1^2}{e^2 \quad F_0^2} \tag{S5}$$

In the equations above the integral F_j is defined by

$$F_j(\eta) = \int_0^\infty \frac{\xi^j d\xi}{1 + e^{(\xi - \eta)}} \tag{S6}$$

The single Kane band model:

Assumed that the light band is nonparabolic and the heavy band is parabolic, SKB (single Kane band) model and SPB mode are applied for for light band and heavy band respectively. it should be noted that the rigid band approximation is adopted which assumes that the changing carrier concentration adjusts only the chemical potential position and not the shape or position of the bands.[5]

As for the single Kane band:[4, 9, 10]

The Seebeck coefficient S:

$$S = \frac{k_B}{e}\left[\frac{F_{1-2}^{1}}{F_{1-2}^{0}} - \eta\right] \tag{S7}$$

The carrier concentration n_H:

$$n_H = \frac{1}{3\pi}\left[\frac{8m^* k_B T}{h^2}\right]^{3/2} F_{3/2,0}^{0} \tag{S8}$$

The mobility μ_H:

$$\mu_H = \frac{h^4 e C_{ll} \quad 3F_{1,-2}^{0}}{8\pi^3 m_I^* (2m_b^* k_B T)^{3/2} E_{def}{}^2 F_{3/2,0}^{0}} \tag{S9}$$

Due to the anisotropy of both conduction and valence bands, the inertial effective mass m_I^*, and the density of states effective mass m^* are governed by the effective band mass

of a single pocket along two directions $m_{//}^*$ and $m_{\perp}^*$:[11]

$$m^* = N_V^{2/3} m_b^* = N_V^{\frac{2}{3}} (m_{\perp}^{*2} m_{\parallel}^{*2})^{1/3}; \quad m_I^* = 3(\frac{2}{m_{\perp}^*} + \frac{1}{m_{\parallel}^*})^{-1}. \tag{S10}$$

where N_V is the band degeneracy (N_{V1}=4 for the light-mass valence band, N_{V2}=12 for the heavy-mass valence band of SnTe. [12]

The Hall factor A:

$$A = \frac{3K(K+2)F_{1/2,-4}^{0} F_{3/2,0}^{0}}{(2K+1)^2 \quad (F_{1,-2}^{0})^2} \tag{S11}$$

where $K=m_{\parallel}^*/m_{\perp}^*$ (K=4, assumed T independent), which reflects the anisotropy of the energy band.[8]

The Lorenz number L:

$$L = (\frac{k_B}{e})^2 [\frac{F_{1,-2}^{2}}{F_{1,-2}^{0}} - (\frac{F_{1,-2}^{1}}{F_{1,-2}^{0}})^2] \tag{S12}$$

In the equations above the integral $F_{m,n}^{l}$ is defined by

$$F_{m,n}^{l} = \int_0^{\infty} (-\frac{\partial f}{\partial \varepsilon}) \varepsilon^l (\varepsilon + \beta\varepsilon^2)^m [(1+2\beta\varepsilon)^2 + 2]^{1/2} d\varepsilon \tag{S13}$$

where $\beta = \frac{k_B T}{E_g}$ ($E_g$is the band gap) is the reciprocal reduced band gap, is the nonparabolicity parameter.

Relaxation Time Model for Carrier Scattering：[13]

In heavily heterovalently doped semiconductors, acoustic phonon-dominated deformation potential scattering is often not the only dominant role in carrier scattering. Alloy scattering, polar scattering, ionized impurity scattering, and inter-valley scattering also play an important role. Herein, acoustic phonon scattering, polar scattering, alloy scattering and together with ionized impurity scattering, with the total relaxation time determined by Matthiessen's rule, are considered to understand the transport properties of Sb_2Te_3 alloying and Cd doping:

$$\tau_{total}^{-1} = \tau_{ac}^{-1} + \tau_{po}^{-1} + \tau_{al}^{-1} + \tau_{ii}^{-1} \tag{S14}$$

The relaxation time for acoustic phonon scattering based on deformation potential theory can be expressed:[8]

$$\tau_{ac}(\varepsilon) = \frac{\pi\hbar^4 v_l^2 \rho N_v}{2^{\frac{1}{2}} m_d^{*3/2} (k_B T)^{\frac{3}{2}} E_{def}^2} (\varepsilon + \varepsilon^2\beta)^{-\frac{1}{2}} (1+2\beta\varepsilon)^{-1} [1 - \frac{8\beta(\varepsilon+\varepsilon^2\beta)}{3(1+2\beta\varepsilon)^2}]^{-1} \tag{S15}$$

where v_l is the longitudinal velocity, ρ is the density.

For SnTe, a typical polar molecule, carriers are also scattered due to the change in polarity caused by optical vibrations. At room temperature and above, polar scattering from optical phonons can be viewed as an elastic process whose relaxation time can be defined as:[14]

$$\tau_{po}(\varepsilon) = \frac{4\pi\hbar^2\varepsilon^{1/2}N_v^{1/3}}{2^{\frac{1}{2}}m_d^{*1/2}(k_BT)^{\frac{1}{2}}e^2(\varepsilon_\infty^{-1} - \varepsilon_0^{-1})}(1 + \varepsilon\beta)^{\frac{1}{2}}(1 + 2\beta\varepsilon)^{-1}\left\{\left[1 - \delta\ln\left(1 + \frac{1}{\delta}\right)\right] - \frac{2\beta(\varepsilon + \varepsilon^2\beta)}{(1 + 2\beta\varepsilon)^2}[1 - 2\delta + 2\delta^2\ln[\right.$$

(S16)

where ε_∞ and ε_0 are the high frequency and static dielectric constants, respectively. δ is a function of reduced carrier energy ε defined as:

$$\delta(\varepsilon) = \frac{e^2m_d^{*\frac{1}{2}}N_v^{\frac{2}{3}}}{2^{\frac{1}{2}}\varepsilon(k_BT)^{\frac{1}{2}}\pi\hbar\varepsilon_\infty}(1 + \varepsilon\beta)^{-1}F_{\frac{1}{2},1}^{0} \quad \text{(S17)}$$

The relaxation time of alloy disorder is mainly determined by the macroscopic uniform crystal structure changes caused by its alloying and doping atoms, which can be expressed as:[15]

$$\tau_{al}(\varepsilon) = \frac{8\hbar^4}{3\sqrt{2}\pi\Omega x(1 - x)m_b^{*\frac{3}{2}}(k_BT)^{\frac{1}{2}}E_{al}^2}(\varepsilon + \varepsilon^2\beta)^{-\frac{1}{2}}(1 + 2\beta\varepsilon)^{-1}\left[1 - \frac{8\beta(\varepsilon + \varepsilon^2\beta)}{3(1 + 2\beta\varepsilon)^2}\right]^{-1} \quad \text{(S18)}$$

Where Ω is the volume per atom, x is the concentration ratio of the alloy atom, E_{al} is the alloy scattering potential which determines the magnitude of the alloy scattering.[16, 17]

$$\tau_{ii}(\varepsilon) = \frac{4\sqrt{2}\pi\varepsilon_0^2m_d^{*1/2}(k_BT)^{\frac{3}{2}}}{N_{ii}Z^2e^4}\varepsilon^{3/2}(1 + \varepsilon\beta)^{3/2}(1 + 2\beta\varepsilon)^{-1}\left[\ln(1 + b) - \frac{b}{1 + b}\right]^{-1} \quad \text{(S19)}$$

$$b = \frac{2^{3/2}\pi^2\varepsilon_0\hbar(k_BT)^{1/2}}{m_d^{*1/2}e^2}\frac{\varepsilon}{F_{-\frac{1}{2}}(\eta)} \quad \text{(S20)}$$

where N is amount of impurities per unit volume, Z represents the Z effective charges.

Therefore, the carrier mobility μ can be expressed as:

$$\mu = \frac{e \int_0^{\infty} (-\frac{\partial f}{\partial \varepsilon}) \tau_{total} (\varepsilon + \varepsilon^2\beta)^{3/2} (1 + 2\beta\varepsilon)^{-1} d\varepsilon}{m_I^* \int_0^{\infty} (-\frac{\partial f}{\partial \varepsilon}) (\varepsilon + \varepsilon^2\beta)^{3/2} d\varepsilon} \tag{S21}$$

The Seebeck coefficient S:

$$S = \frac{k_B}{e} \left(\frac{\int_0^{\infty} \left(-\frac{\partial f}{\partial \varepsilon}\right) \tau_{total} \varepsilon^{\frac{3}{2}} (\varepsilon + \varepsilon^2\beta)^{3/2} (1 + 2\beta\varepsilon)^{-1} d\varepsilon}{\int_0^{\infty} \left(-\frac{\partial f}{\partial \varepsilon}\right) \tau_{total} \varepsilon^{\frac{1}{2}} (\varepsilon + \varepsilon^2\beta)^{\frac{2}{3}} (1 + 2\beta\varepsilon)^{-1} d\varepsilon} - \eta \right) \tag{S22}$$

The Hall coefficient A:

$$A = \frac{3K(K+2) \int_0^{\infty} \left(-\frac{\partial f}{\partial \varepsilon}\right) \tau_{total} \varepsilon^{\frac{3}{2}} (1 + \varepsilon\beta)^{\frac{3}{2}} (1 + 2\beta\varepsilon)^{-2} d\varepsilon \int_0^{\infty} \left(-\frac{\partial f}{\partial \varepsilon}\right) \tau_{total} \varepsilon^{\frac{3}{2}} (1 + \varepsilon\beta)^{\frac{3}{2}} d\varepsilon}{(2K+1)^2 \left(\int_0^{\infty} \left(-\frac{\partial f}{\partial \varepsilon}\right) \tau_{total} \varepsilon^{\frac{1}{2}} (\varepsilon + \varepsilon^2\beta)^{3/2} (1 + 2\beta\varepsilon)^{-1} d\varepsilon \right)^2} \tag{S23}$$

And the Lorenz number L:

$$L = \left(\frac{k_B}{e}\right)^2 \left[\frac{\int_0^{\infty} \left(-\frac{\partial f}{\partial \varepsilon}\right) \tau_{total} \varepsilon^{\frac{7}{2}} (1 + \varepsilon\beta)^{\frac{3}{2}} (1 + 2\beta\varepsilon)^{-1} d\varepsilon}{\int_0^{\infty} \left(-\frac{\partial f}{\partial \varepsilon}\right) \tau_{total} \varepsilon^{\frac{3}{2}} (1 + \varepsilon\beta)^{\frac{2}{3}} (1 + 2\beta\varepsilon)^{-1} d\varepsilon} - \left(\frac{\int_0^{\infty} \left(-\frac{\partial f}{\partial \varepsilon}\right) \tau_{total} \varepsilon^{\frac{5}{2}} (1 + \varepsilon\beta)^{\frac{3}{2}} (1 + 2\beta\varepsilon)^{-1} d\varepsilon}{\int_0^{\infty} \left(-\frac{\partial f}{\partial \varepsilon}\right) \tau_{total} \varepsilon^{\frac{3}{2}} (1 + \varepsilon\beta)^{\frac{2}{3}} (1 + 2\beta\varepsilon)^{-1} d\varepsilon} \right)^2 \right] \tag{S24}$$

The two valence band model:

It should be noted that the relative positions of the Fermi level and the two valence bands need to be considered when using the two-band model. That is, the difference between the reduced chemical potentials corresponding to the two valence bands $\Delta = \frac{\Delta E}{k_B T}$.[4, 10] And the total electrical conductivity:

$$\sigma = \sigma_L + \sigma_\Sigma \tag{S25}$$

The total Seebeck coefficient:

$$S = \frac{S_L \sigma_L + S_\Sigma \sigma_\Sigma}{\sigma_L + \sigma_\Sigma} \tag{S26}$$

The total Lorenz number:

$$L = \frac{L_L\sigma_L + L_\Sigma\sigma_\Sigma}{\sigma_L + \sigma_\Sigma} \tag{S27}$$

The total carrier concentration n_H:

$$n_H = \frac{[bn_{LH} + n_{\Sigma H}]^2}{A_{LH}b^2n_{LH} + A_{\Sigma H}n_{\Sigma H}} \tag{S28}$$

where b=4, that is suitable for PbTe/SnTe system.

The total Hall coefficient R_H:

$$R_H = \frac{\sigma_L^2R_{LH} + \sigma_\Sigma^2R_{\Sigma H}}{(\sigma_L + \sigma_\Sigma)^2} \tag{S29}$$

The total Hall mobility μ_H:

$$\mu_H = R_H\sigma \tag{S30}$$

Debye-Callaway Model Simulation

According to the Debye-Callaway model, [18, 19] κ_L can be calculated by

$$\kappa_L = \frac{K_B}{2\pi^2\upsilon}\left(\frac{K_B}{\hbar}\right)^3\int_0^{\Theta/T}\tau(x)\frac{x^4e^x}{(e^x - 1)^2}dx \tag{S7}$$

The integrand item in conjunction with the coefficient of the above equation is the spectral lattice thermal conductivity (κ_s), [20, 21] can be given by:

$$\kappa_s = \frac{k_B}{2\pi^2\upsilon}\left(\frac{k_B}{\hbar}\right)^3\tau(x)\frac{x^4e^x}{(e^x - 1)^2} \tag{S8}$$

Where $v = 3^{1/3}(v_l^{-3} + 2v_t^{-3})^{-1/3}$ (with v_l and v_t respectively denoting the transverse and longitudinal sound velocities) is the average speed of phonon, $x = \hbar\omega/k_BT$ (with ω denoting the phonon frequency) is the reduced phonon frequency, Θ is Debye temperature, $\hbar$ is the reduced Planck constant, k_B is the Boltzmann constant, and τ_{tot} is the total relaxation time. The phonon scattering pathways include Umkalapp (U) phonon scattering, normal process (N), point defects (PD), and others.The relevant phonon relaxation times are given by:

Umklapp phonon scattering and Normal process

$$\tau_U^{-1} = \frac{\hbar\omega^2\gamma^2T}{Mv^2\Theta}e^{-\Theta/T} \tag{S9}$$

Normal process τ_N^{-1}:

$$\tau_N^{-1} = \beta\tau_U^{-1} \quad \text{(S12)}$$

Point defect phonon scattering

$$\tau_{PD}^{-1} = \frac{V_0}{4\pi^2 \upsilon}\Gamma\omega^4 \quad \text{(S12)}$$

where M is the average atomic mass, γ is the Grüneisen parameter, β is the ratio between normal process and Umklapp phonon scattering, V_0 is the average atomic volume, Γ is the point defect scattering parameter. Remarkably, the disorder scattering parameter Γ can be derived from the model of Slack and by Abeles assuming $\Gamma = \Gamma_M + \Gamma_S$,[22, 23] where the scattering parameters Γ_M and Γ_S are due to mass and strain field fluctuations, respectively. The mass and strain fluctuation scattering parameter is given by:

$$\Gamma_M = \frac{\sum_{i=1}^{n} c_j(\bar{M}_i/\bar{\bar{M}})^2 f_i^1 f_i^2 [(M_i^1 - M_i^2)/\bar{M}_i]^2}{\sum_{i=1}^{n} c_i} \quad \text{(S28)}$$

$$\Gamma_S = \frac{\sum_{i=1}^{n} c_j(\bar{M}_i/\bar{\bar{M}})^2 f_i^1 f_i^2 \varepsilon[(r_i^1 - r_i^2)/\bar{r}_i]^2}{\sum_{i=1}^{n} c_i} \quad \text{(S29)}$$

where n, c_j, $\bar{M}_i$, $\bar{\bar{M}}$, M_i^k, r_i^k, f_i^k and ε are the number of sublattice, the relative degeneracies of the respective sites, the average atomic mass of the ith sublattice, the average atomic mass of the compound, the atomic mass of the kth atom of the ith sublattice, the atomic radius of the kth atom of ith sublattice, the fractional concentrations of kth atom of the ith sublattice and the lattice inharmonic parameter, respectively. In particular, the mass of the Sn vacancy is estimated to be 0, and the radius is 0.5-0.6 of the ionic radius of Sn.

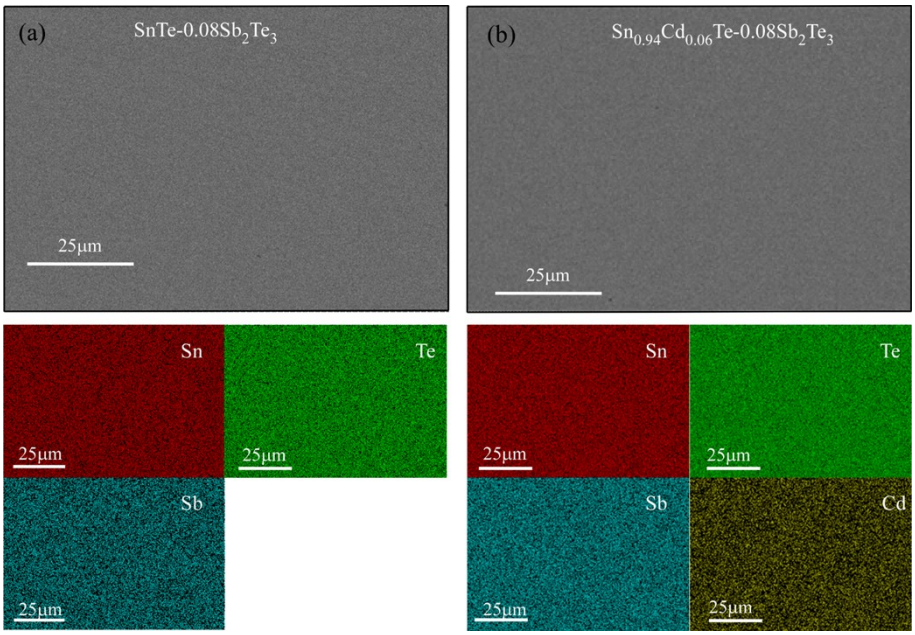

Fig. S1. Backscattered electron (BSE) images and corresponding elemental mappings (EDS) of carefully polished surfaces for (a) $SnTe\text{-}0.08Sb_2Te_3$ and (b) $Sn_{0.94}Cd_{0.06}Te\text{-}0.08Sb_2Te_3$.

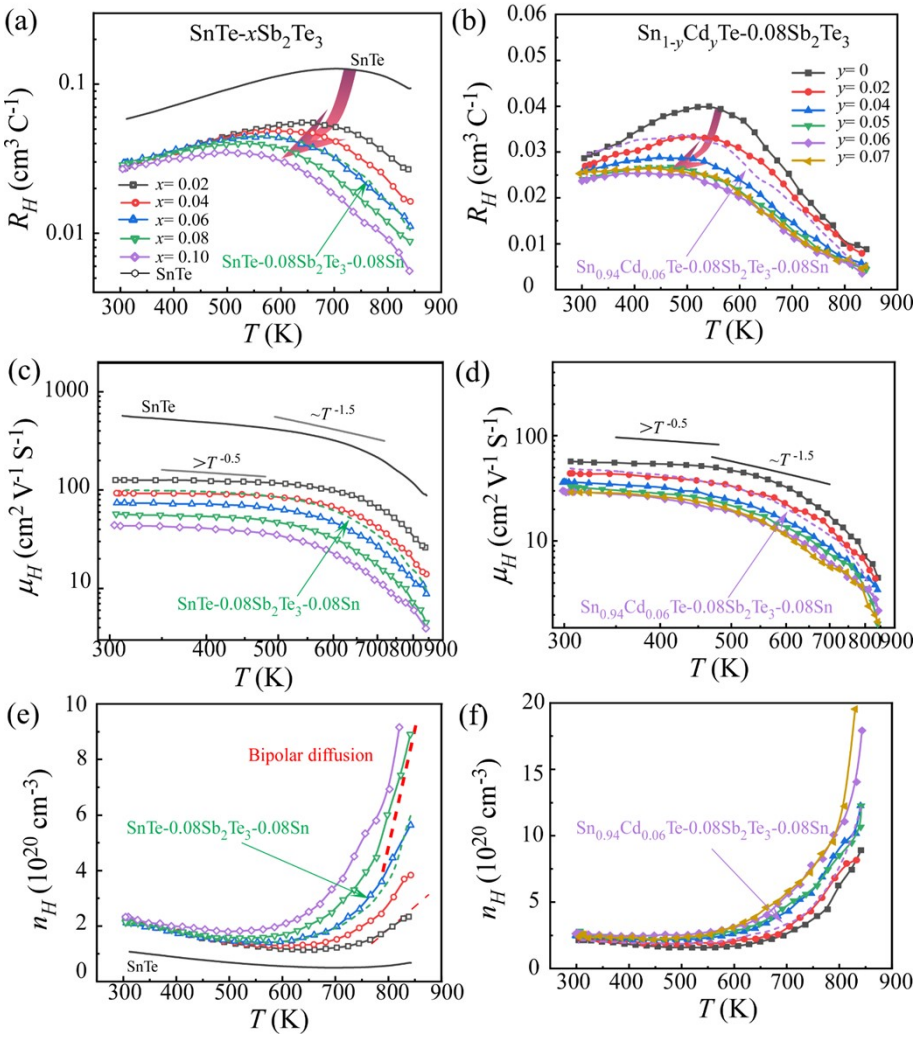

Fig. S2. Temperature dependence of (a, b) Hall coefficients, (c, d) carrier mobility and (e, f) carrier concentration for (a, c, e) SnTe-$x$$Sb_2Te_3$ (x = 0, 0.02, 0.04, 0.06, 0.08, 0.1) and (b, d, f) $Sn_{1-y}Cd_yTe$-0.08Sb_2Te_3 (y = 0.02, 0.04, 0.05, 0.06, 0.07).

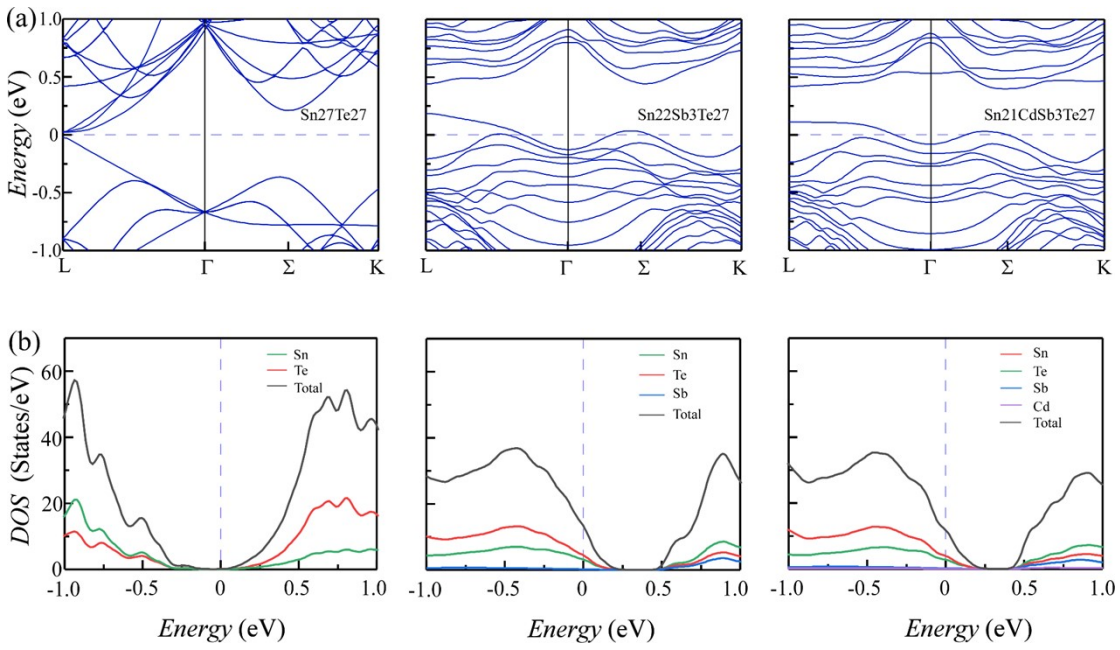

Fig. S3. (a) Electronic band structures of $Sn_{27}Te_{27}$, $Sn_{22}V_2Sb_3Te_{27}$ and $Sn_{21}V_2CdSb_3Te_{27}$ supercells as a function of wave vector in the Brillouin zone; (b) Density of states (DOS) of $Sn_{27}Te_{27}$, $Sn_{22}V_2Sb_3Te_{27}$ and $Sn_{21}V_2CdSb_3Te_{27}$ supercells, V is the vacancy.

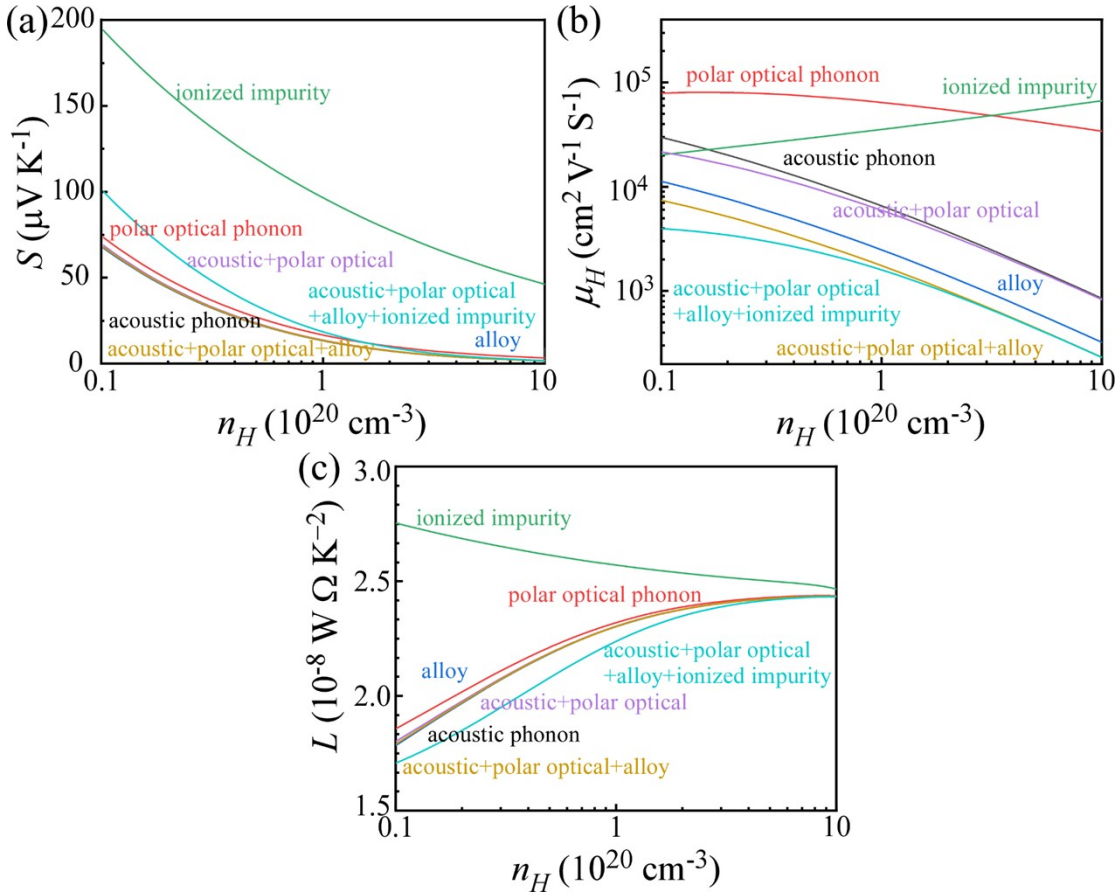

Fig. S4. Taking single-band transport as an example, the changes of (a) Seebeck coefficient S, (b) carrier mobility μ_H and (c) Lorentz number L by carrier scattering mechanisms such as acoustic

phonon scattering, optical polar scattering, alloy scattering and ionized impurity scattering.

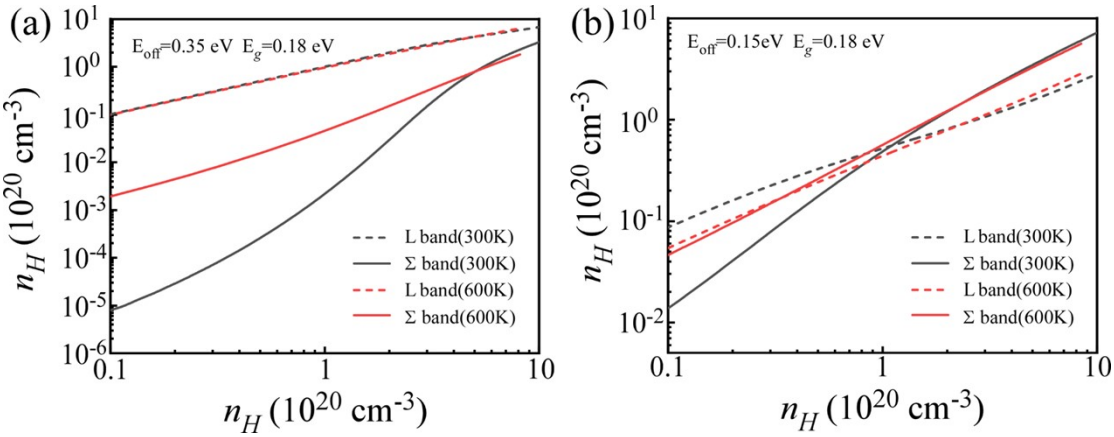

Fig. S5. Carrier distributions of SnTe *L*-band and *Σ*-band in (a) non-converged and (b) converged states, the gray line represents 300 K, and the red line represents a higher temperature of 600 K.

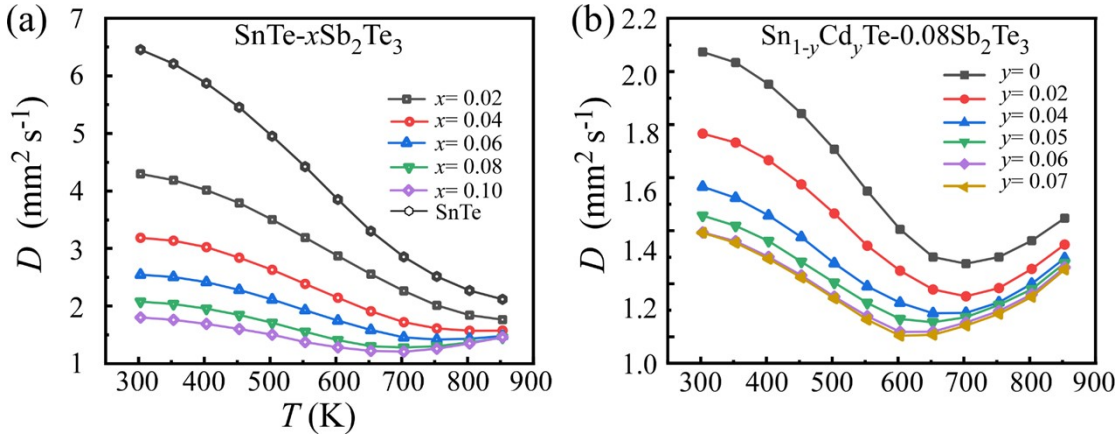

Fig. S6. (a) Temperature dependent thermal diffusivity *D* for (a) SnTe-xSb$_2$Te$_3$ (x = 0, 0.02, 0.04, 0.06, 0.08, 0.1) and (b) Sn$_{1-y}$Cd$_y$Te-0.08Sb$_2$Te$_3$ (y = 0.02, 0.04, 0.05, 0.06, 0.07).

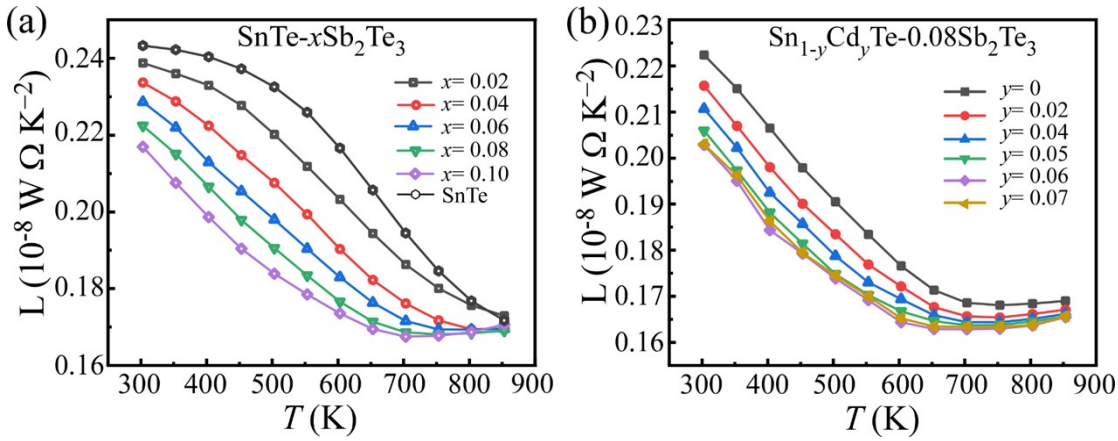

Fig. S7. (a) Temperature dependent Lorenz number *L* for (a) SnTe-xSb$_2$Te$_3$ (x = 0, 0.02, 0.04, 0.06, 0.08, 0.1) and (b) Sn$_{1-y}$Cd$_y$Te-0.08Sb$_2$Te$_3$ (y = 0.02, 0.04, 0.05, 0.06, 0.07).

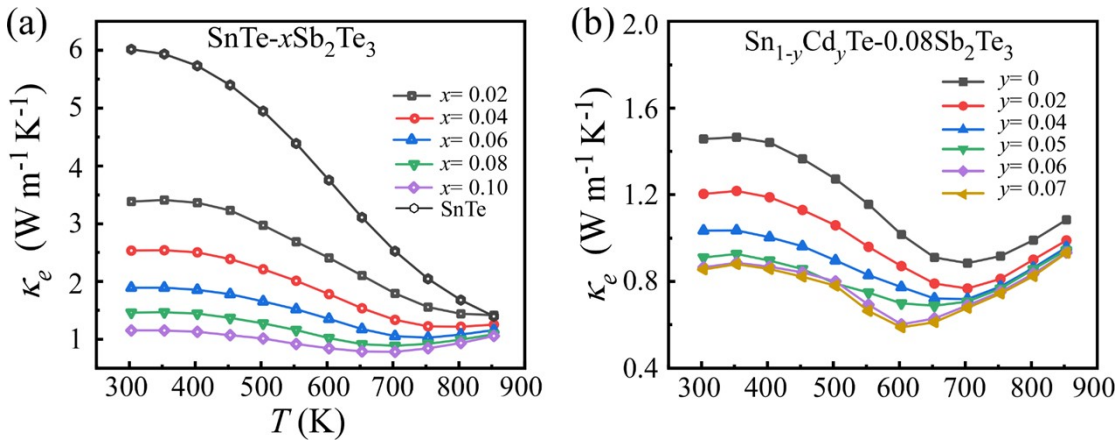

Fig. S8. Temperature dependent electronic thermal conductivity κ_e for (a) SnTe-xSb$_2$Te$_3$ (x = 0, 0.02, 0.04, 0.06, 0.08, 0.1) and (b) Sn$_{1-y}$Cd$_y$Te-0.08Sb$_2$Te$_3$ (y = 0.02, 0.04, 0.05, 0.06, 0.07).

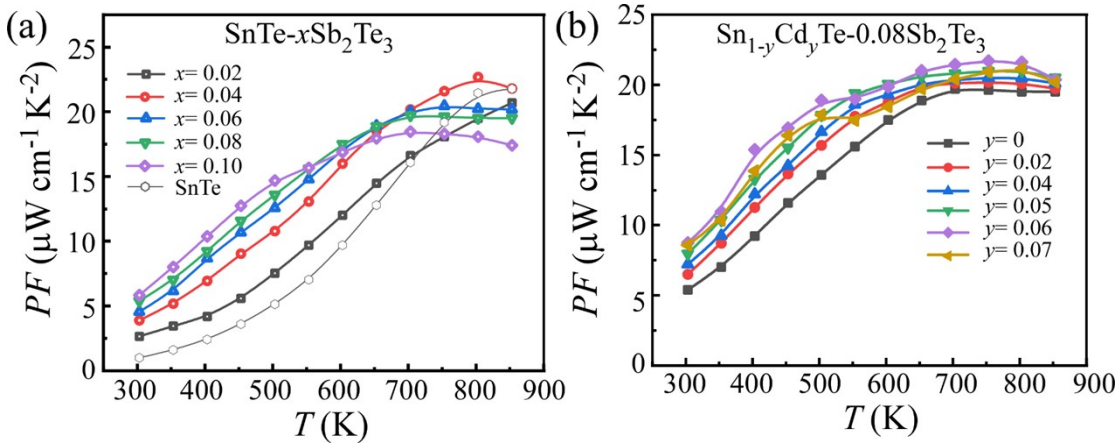

Fig. S9. Temperature dependent power factor *PF* for (a) SnTe-xSb$_2$Te$_3$ (x = 0, 0.02, 0.04, 0.06, 0.08, 0.1) and (b) Sn$_{1-y}$Cd$_y$Te-0.08Sb$_2$Te$_3$ (y = 0.02, 0.04, 0.05, 0.06, 0.07).

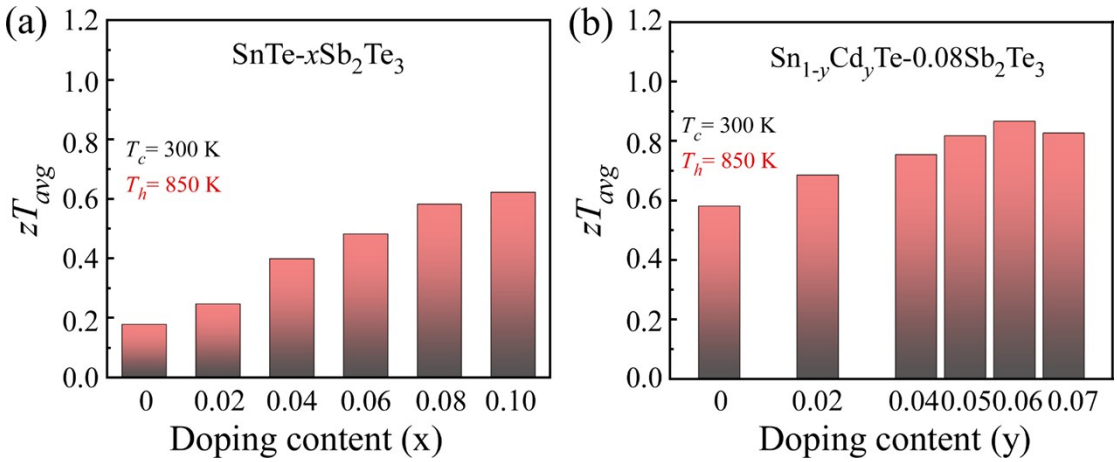

Fig. S10. The average thermoelectric figure of merit zT_{avg} for (a) SnTe-xSb$_2$Te$_3$ (x = 0, 0.02, 0.04, 0.06, 0.08, 0.1) and (b) Sn$_{1-y}$Cd$_y$Te-0.08Sb$_2$Te$_3$ (y = 0.02, 0.04, 0.05, 0.06, 0.07) between 303K and 853K.

Table S2. Parameters used to calculate carrier transport of SnTe based on two band model.

Paramaters	Values
Combination of elastic constants C_l (Pa)	5.8×10^{10}
Ratio of the longitudinal to transverse band effective mass K_L	4 [4]
Ratio of the longitudinal to transverse band effective mass K_Σ	1 [4]
Band gap E_g (eV)	$0.054+4.2\times10^{-4}\times T$ [24]
Energy offset ΔE (eV)	$0.45-2.5\times10^{-4}\times T$ [25]
Band effective mass of V_L m_b^* (m_0)	$e^{lg0.17 + 0.5lg\frac{T}{300}}$
Band effective mass of V_Σ m_b^* (m_0)	1.92
Deformation potential of V_L E_{def} (eV)	35 (this work)
Deformation potential of V_Σ E_{def} (eV)	25 (this work)
Light valence Band degeneracy N_L	4
heavy valence Band degeneracy N_Σ	12

Table S3. Parameters adopted in the Debye-Callaway Model Simulation.

Parameters	Values
Longitudinal sound velocity v_L (m s^{-1})	3171[26]
Transverse sound velocity v_T (m s^{-1})	1220[26]
Sound velocity v (m s^{-1})	1967
Atomic mass Sn (kg)	1.97×10^{-25}
Atomic mass Te (kg)	2.12×10^{-25}
Atomic mass Sb (kg)	2.02×10^{-25}
Atomic mass Cd (kg)	1.87×10^{-25}
Atomic mass vacancy (kg)	0
Ionic radius Sn (Å)	0.93
Ionic radius Te (Å)	2.11
Ionic radius Sb (Å)	0.76
Ionic radius Cd (Å)	0.97
Ionic radius vacancy (Å)	50% $r_{Sn^{2+}}$
Grüneisen parameter γ	2.2[27-29]
Point defect scattering parameters Γ	(fitted)

Temperature-dependent ratio of normal phonon scattering to Umklapp scattering	β	2.3 (fitted)

References:

1 R. Blachnik and R. Igel, *Zeitschrift für Naturforschung B*, 1974, **29**, 625-629.

2 Y. Pei, X. Shi, A. LaLonde, H. Wang, L. Chen and G. J. Snyder, *Nature*, 2011, **473**, 66-69.

3 H.-S. Kim, Z. M. Gibbs, Y. Tang, H. Wang and G. J. Snyder, *APL Mater.*, 2015, **3**, 041506.

4 M. Hong, Y. Wang, S. Xu, X. Shi, L. Chen, J. Zou and Z.-G. Chen, *Nano Energy*, 2019, **60**, 1-7.

5 M. Zhou, Z. M. Gibbs, H. Wang, Y. Han, C. Xin, L. Li and G. J. Snyder, *Phys. Chem. Chem. Phys.*, 2014, **16**, 20741-20748.

6 Y. Xiao, H. Wu, W. Li, M. Yin, Y. Pei, Y. Zhang, L. Fu, Y. Chen, S. J. Pennycook, L. Huang, J. He and L. D. Zhao, *J. Am. Chem. Soc.*, 2017, **139**, 18732-18738.

7 T. Seddon and S. C. Gupta, *Solid State Commun*, 1976, **20**, 69-72.

8 C. Herring and E. Vogt, *Phys. Rev.*, 1956, **101**, 944-961.

9 Y. Pei, Z. M. Gibbs, A. Gloskovskii, B. Balke, W. G. Zeier and G. J. Snyder, *Adv. Energy Mater.*, 2014, **4**, 1400486.

10 Q. Zhang, B. Liao, Y. Lan, K. Lukas, W. Liu, K. Esfarjani, C. Opeil, D. Broido, G. Chen and Z. Ren, *Proc. Natl. Acad. Sci. U.S.A.*, 2013, **110**, 13261–13266.

11 Y. Pei, A. D. LaLonde, H. Wang and G. J. Snyder, *Energy Environ. Sci.*, 2012, **5**, 7963-6969.

12 L. M. ROGERS, *J. Phys. D Appl. Phys.*, 1963, **1**, 845-852.

13 H. Xie, H. Wang, C. Fu, Y. Liu, G. J. Snyder, X. Zhao and T. Zhu, *Sci. Rep.*, 2014, **4**, 6888.

14 V. I. Fistul, *Heavily doped Semiconductor*, 1969, New York, Plenum Press.

15 J. W. harrison and T. R. Hauser, *Phys. Rew. B*, 1976, **13**, 5347.

16 X. Liu, T. Zhu, H. Wang, L. Hu, H. Xie, G. Jiang, G. J. Snyder and X. Zhao, *Adv. Energy Mater.*, 2013, **3**, 1238-1244.

17 H. Xie, H. Wang, Y. Pei, C. Fu, X. Liu, G. J. Snyder, X. Zhao and T. Zhu, *Adv. Funct. Mater.*, 2013, **23**, 5123-5130.

18 D. Bessas, I. Sergueev, H.-C. Wille, J. Perßon, D. Ebling and R. Hermann, *Physical Review B*, 2012, **86**, 224301.

19 J. Callaway and H. C. von Baeyer, *Physical Review*, 1960, **120**, 1149.

20 J. Callaway, *Phys. Rev.*, 1959, **113**, 1046-1051.

21 H. Wang, T. Wang, J. Hwang, W. Su, H. Kim, J. Zhai, X. Wang, C. Wang and W. Kim, *Inorg. Chem. Front.*, 2018, **5**, 793-801.

22 G. A. Slack, *Phys. Rew.*, 1957, **105**, 829-831.

23 B. Abeles, *Phys. Rev.*, 1963, **131**, 1906-1911.

24 G. Tan, L.-D. Zhao, F. Shi, J. W. Doak, S.-H. Lo, H. Sun, C. Wolverton, V. P. Dravid, C. Uher and M. G. Kanatzidis, *J. Am. Chem. Soc.*, 2014, **136**, 7006-7017.

25 M. Zhou, Z. M. Gibbs, H. Wang, Y. Han, C. Xin, L. Li and G. J. Snyder, *PCCP*, 2014, **16**, 20741-20748.

26 R. Moshwan, W. D. Liu, X. L. Shi, Y. P. Wang, J. Zou and Z. G. Chen, *Nano Energy*, 2019, **65**, 104056.

27 H. C. Wang, T. Wang, J. Hwang, W. B. Su, H. Kim, J. Z. Zhai, X. Wang, C. L. Wang and W. Kim, *Inorg. Chem. Front*, 2018, **5**, 793-801.

28 R. Al Rahal Al Orabi, N. A. Mecholsky, J. Hwang, W. Kim, J.-S. Rhyee, D. Wee and M. Fornari,

Chem. Mater., 2015, **28**, 376-384.

29 C. Toher, J. J. Plata, O. Levy, M. de Jong, M. Asta, M. B. Nardelli and S. Curtarolo, *Phys. Rev. B*, 2014, **90**, 174107.